SOLUTION MINING RESEARCH INSTITUTE
679 Plank Road
Clifton Park, NY 12065, USA

Telephone: +1 518-579-6587
www.solutionmining.org

Technical Conference Paper

1965 – 2025

SafeInCave:
An Open-Source Simulator for Energy Storage in Heterogeneous Salt Caverns

Hermínio T. Honório, Delft University of Technology, Delft, the Netherlands
Mohammad S. Amin, Delft University of Technology, Delft, the Netherlands
Lucas Landeweerd, Delft University of Technology, Delft, the Netherlands
Hadi Hajibeygi, Delft University of Technology, Delft, the Netherlands

SMRI Fall 2025 Technical Conference
29-30 September 2025
Wichita, Kansas, United States

Solution Mining Research Institute Fall 2025 Technical Conference

Wichita, Kansas, United States 29-30 September 2025

SAFEINCAVE: AN OPEN-SOURCE SIMULATOR FOR ENERGY STORAGE IN HETEROGENEOUS SALT CAVERNS

Hermínio T. Honório, Mohammad S. Amin, Lucas Landeweerd, and Hadi Hajibeygi

Delft University of Technology, Delft, the Netherlands

Abstract

Utilization of salt caverns for underground gas storage (UGS), including hydrogen, is expected to increase in the coming years. This scaling up leads to cavern development in more heterogeneous geosystems, even close to the boundary of the salt rock deposits around the porous rock formations. These cases increase the chance of weakening the cavern stability, especially when operated under fast cycles. In face of these concerns, reliable numerical simulation of the mechanical response of heterogeneous salt caverns with complex geometries is key to ensure mechanical stability under different operational conditions. Furthermore, numerical simulations can aid in designing safe cavern abandonment strategies, a crucial phase with high societal concerns.

Although salt cavern simulation is necessary, building trust in the numerical results is a challenging task. The reliability of numerical results depends on many different aspects, such as the choice and calibration of appropriate constitutive models, the use of robust numerical schemes, appropriate domain discretization, initial and boundary conditions, etc. “SafeInCave” is an open-source simulator developed to address these aspects. It contains an efficient framework to design, test and calibrate constitutive models for salt rocks in triaxial tests. The current constitutive models include transient creep, reverse transient creep, and steady-state creep (dislocation and pressure solution). The constitutive models are also implemented in a robust 3D finite element simulator. The numerical formulation is specifically developed to (i) easily incorporate new constitutive models, and (ii) provide accurate results for tetrahedral meshes, which are able to efficiently represent complex cavern shapes and geological structures. Finally, a thermodynamic model for brine allows for cavern abandonment simulations. The capabilities and practical applications of SafeInCave are presented and discussed in this work.

Key words: Computer Software, Caverns for Gas Storage, Abandonment, Modeling, Model Calibration, Rock Mechanics

Introduction

Underground gas storage (UGS) in salt caverns has been widely applied for natural gas and is now gaining attention as a key technology to enable large-scale hydrogen storage. The unique properties of rock salt, including low permeability, self-healing capacity, and favourable creep behaviour, make salt caverns particularly suitable for this purpose. With the expected growth in energy storage demand, new caverns are increasingly being developed in heterogeneous geological settings, often near the boundaries of salt deposits or in contact with porous formations. These scenarios present additional challenges to cavern stability, especially under fast pressure cycling and during the abandonment phase, where long-term safety is a primary societal concern (Buzogany, 2022).

Numerical simulation provides a powerful means to analyse the thermo-mechanical response of salt caverns under varying operational and geological conditions. However, building confidence in numerical

predictions requires careful consideration of several aspects, inclusing appropriate constitutive modelling of salt rocks, robust numerical formulations, and discretization strategies capable of handling complex cavern geometries. Many well-established commercial tools are available for this purpose, such as FLAC2D (and 3D), Abaqus, Locas, etc. Despite the importance of these tools, having a fully open-source alternative is essential for the scientific community in many aspects, as it promotes transparency and verifiability, reproducibility of results, extensibility to new models and methods, collaborative development, educational value, etc.

In this context, we present SafeInCave, an open-source simulator specifically designed for the analysis of salt cavern behaviour. SafeInCave provides a modular framework for constitutive model calibration based on triaxial tests and incorporates advanced creep models, including transient, reverse transient, and steady-state creep mechanisms. The simulator is built on a robust finite element formulation optimized for tetrahedral meshes, enabling accurate representation of heterogeneous systems and irregular cavern geometries. In addition, a thermodynamic brine model allows for reliable assessment of cavern abandonment strategies. This paper introduces the main features of SafeInCave and demonstrates its applicability to practical scenarios of energy storage and abandonment of salt caverns.

Salt rock mechanics

For analyzing mechanical stability in salt caverns, it is important to understand how salt rocks deform and how/when they fail. When subjected to a constant non-zero deviatoric stress, salt rocks are observed to continuously deform over time due to creep. It is well known that creep occurs in three stages, namely, transient (primary) creep, steady-state (secondary) creep, accelerated (tertiary) creep. As illustrated in Fig. 1, if the stress condition lies in the compressibility region, the material presents transient and steady-state creep, but no tertiary creep is developed, hence the material continuously deform without failure. By increasing the deviatoric stress (or the von Mises stress q), the salt rocks crosses the compressibility/dilatancy (C/D) boundary and starts to operate in the dilatancy region, where microcracks are created, leading to tertiary creep and subsequent failure. Because the material does not immediately fail, the C/D boundary is also called “long-term” failure boundary. Finally, if the stress condition hits the short-term failure boundary, also depicted in Fig. 1, brittle failure is immediately observed.

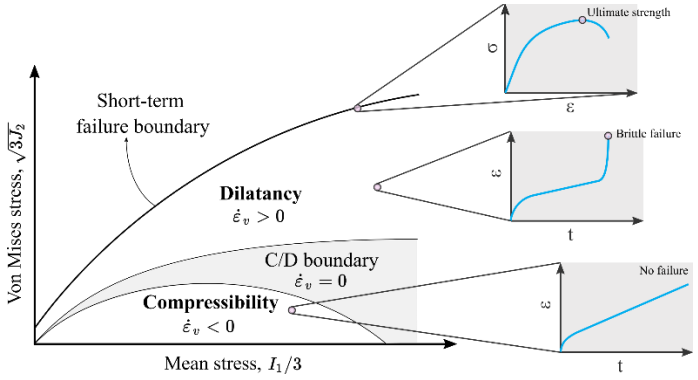

Figure 1 - Compressibility and dilatancy regions for salt rocks.

From the point of view of mechanical stability, the diagram depicted in Fig. 1 suggests that all points around the salt cavern should operate in the compressibility region, as it is far from the short-term failure boundary and no tertiary creep is developed there.

Constitutive model

The constitutive model implemented in the SafeInCave simulator has been developed based on experimental data from cyclic loading triaxial tests performed in salt rock samples. Figure 2 shows one the experimental results in which the radial stress (confining pressure) is kept constant while the axial stress is

applied in a cyclic way. The radial and axial strains are measured and shown in the left graph of the figure. There are two important observations in these results. The first one is illustrated in the middle diagram, which shows the axial stress increasing at a constant rate from point A to B (blue), while the axial strain (red) increases approximately at a constant rate from A' to B'. However, when the stress goes from point B to C, the axial strain suddenly increases from B' to C', as if an additional deformation mechanism is triggered when the stress level exceeds a threshold. In the figure, the threshold is 31 MPa, which is the maximum axial stress ever experienced by the salt rock at that point. This is observed in every stress cycle during the experiment. It is also possible to verify that the axial strain continues to develop after the axial strain becomes constant at 33.5 MPa, which characterizes a transient creep deformation. The second observation relates to the stress-strain curve during the unloading/reloading steps, as depicted in the rightmost graph in Fig. 2. The hysteretic effect from B''-A'' and A''-B'' characterizes the so-called reverse transient creep, which is usually depicted in the strain vs. time graph during an unloading step (see Figure 3, for example). Finally, the volumetric strain shown in Fig.1 is always positive during the experiment. This indicates that the salt sample operates in the compressibility region during the entire experiment, thus reproducing the ideal condition for salt cavern operations.

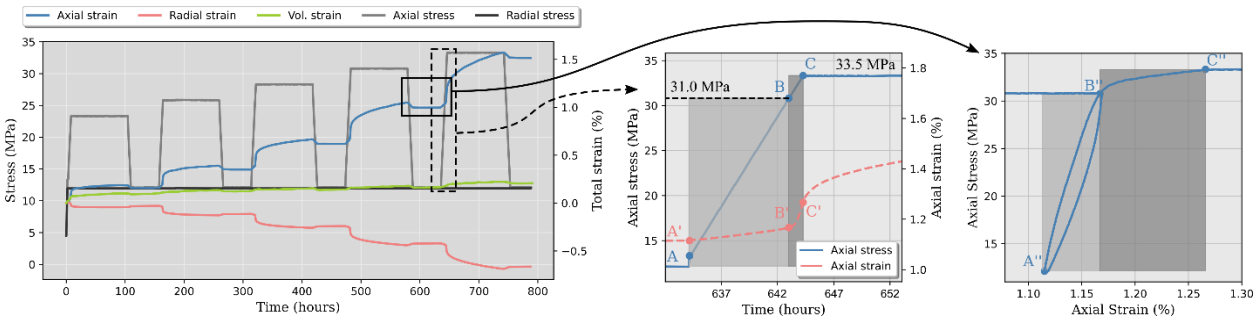

Figure 2 - Experimental data from salt rock triaxial test performed under cyclic loading condition (Honório *et al*, 2024).

In addition to transient and reverse transient creep, the total strains shown in Fig. 2 are also composed of dislocation creep, pressure solution creep, and (instantaneous) elastic responses. Although the experiment was performed at constant temperature, thermal strain is also an effect to be considered. Based on these observations, and assuming infinitesimal strains, we compose the constitutive model by adding individual contributions for each deformation mechanism, as illustrated in Fig. 3. A Hookean spring is used to capture instantaneous elastic responses ($\boldsymbol{\varepsilon_e}$); transient creep ($\boldsymbol{\varepsilon_{vp}}$) is described by a viscoplastic model with appropriate yield surface and hardening rule; steady-state creep comprises both dislocation ($\boldsymbol{\varepsilon_{dc}}$) and pressure-solution ($\boldsymbol{\varepsilon_{pc}}$) creep mechanisms; reverse transient creep ($\boldsymbol{\varepsilon_{ve}}$) is captured by a viscoelastic Kelvin-Voigt element (spring in parallel with a dashpot); and thermal strains ($\boldsymbol{\varepsilon_{th}}$) are represented by a ballon that isotropically expands/contracts as a response to temperature variations.

Based on the constitutive model representation of Fig. 3, the total strain can be decomposed as

$$\boldsymbol{\varepsilon} = \boldsymbol{\varepsilon}_e + \underbrace{\boldsymbol{\varepsilon}_{vp} + \boldsymbol{\varepsilon}_{dc} + \boldsymbol{\varepsilon}_{pc} + \boldsymbol{\varepsilon}_{ve}}_{\boldsymbol{\varepsilon}_{ne}} + \boldsymbol{\varepsilon}_{th} = \boldsymbol{\varepsilon}_e + \boldsymbol{\varepsilon}_{ne} + \boldsymbol{\varepsilon}_{th}. \tag{1}$$

where the term $\boldsymbol{\varepsilon}_{ne}$ refers to the "non-elastic" strains, which includes all inelastic and viscoelastic strains. Each contribution in Eq. (1) is briefly described below.

Elastic strain

The elastic response relates to the stress tensor according to Hooke's law, that is,

$$\boldsymbol{\sigma} = \mathbf{C} : \boldsymbol{\varepsilon}_e \tag{2}$$

where $\mathbf{C}$ represents the rank-4 elastic stiffness tensor.

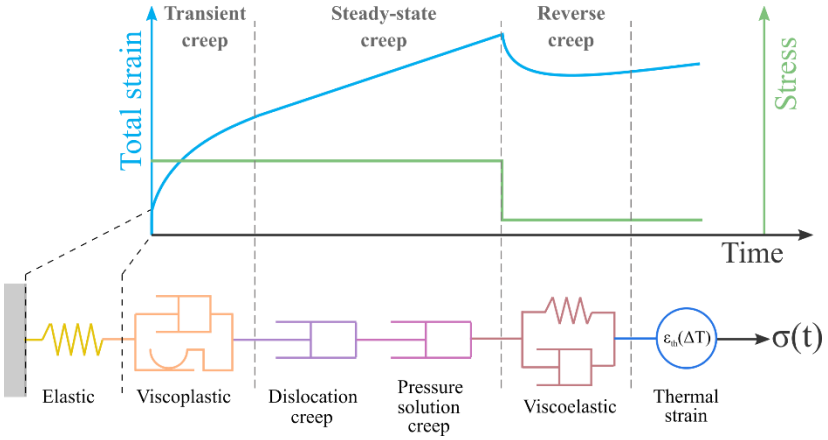

Figure 3 - Constitutive model representation.

Viscoplastic strain rate

Perzyna's formulation is employed for the viscoplastic strain element to describe transient creep. The viscoplastic strain rate is given by

$$\dot{\boldsymbol{\varepsilon}}_{vp} = \mu_1 \left\langle \frac{F_{vp}}{F_0} \right\rangle^N \frac{\partial \mathrm{F_{vp}}}{\partial \boldsymbol{\sigma}}, \tag{3}$$

where μ_1 and N are material parameters, F_0 is a reference value, and the yield surface is given according to Desai's model (Desai and Varadarajan, 1987), which was successfully employed in Khaledi *et al.* (2016) and Honório and Hajibeygi, (2024).

Dislocation creep strain rate

Dislocation creep is a intragrain deformation mechanism that is commonly described by a power law function together with Arrhenius' law for temperature dependency, that is,

$$\dot{\boldsymbol{\varepsilon}}_{dc} = A_{dc} \exp\left(-\frac{Q_{dc}}{RT}\right) q^{n-1} \boldsymbol{s}, \tag{4}$$

where A_{dc}, Q_{dc}, and n are material parameters, R is the universal gas constant, T is temperature in Kelvin, q is the von Mises stress, and $\boldsymbol{s}$ is the deviatoric stress tensor.

Pressure solution creep strain rate

Pressure solution creep occurs at the grain boundaries in the presence of humidity, as described by Spiers *et al.* (1990). The strain rate is inversely proportional to temperature and to the grain size d to the power 3, Arrheniu's law also applies, and it is linearly dependent on the deviatoric stress, that is,

$$\dot{\boldsymbol{\varepsilon}}_{pc} = \frac{A_{pc}}{d^3 T} \exp\left(-\frac{Q_{pc}}{RT}\right) \boldsymbol{s}, \tag{5}$$

where A_{pc} and Q_{pc} are also material parameters.

Viscoelastic strain

A Kelvin-Voigt element is composed of a spring in parallel with a linear dashpot, as illustrated in Fig. 3. The total stress applied to this element is equilibrated by the stresses developed in the dashpot and the spring. In this manner, the viscoelastic strain rate can be computed as

$$\sigma = \mathbf{C}_1 : \boldsymbol{\varepsilon}_{\mathrm{ve}} + \eta \dot{\boldsymbol{\varepsilon}}_{ve} \quad \rightarrow \quad \dot{\boldsymbol{\varepsilon}}_{ve} = \frac{1}{\eta}(\sigma - \mathbf{C}_1 : \boldsymbol{\varepsilon}_{\mathrm{ve}}). \tag{6}$$

Thermal strain

Temperature variations cause the material to expand or shrink in a purely isotropic manner. The thermal strain tensor can be represented as

$$\boldsymbol{\varepsilon}_{th} = \alpha \Delta T \boldsymbol{I}, \tag{7}$$

with α denoting the thermal expansion coefficient, ΔT the temperature variation, and $\boldsymbol{I}$ the rank-2 identity tensor.

Governing equations

This section presents the governing equations considered in the SafeInCave simulator. The following subsections describe the heat diffusion equation, the linear momentum balance equations, and the thermodynamic model for brine (used in salt cavern abandonment simulations).

Heat diffusion equation

The mechanical behavior of materials is primarily described by the linear momentum balance equation. However, since temperature can also have a significant effect on the material mechanics, the energy conservation equation is also necessary. Considering only heat diffusion and no internal heat generation, the energy conservation equation reads

$$\rho c_p \frac{\partial T}{\partial t} - \nabla \cdot (k \nabla T) = 0, \tag{8}$$

where ρ, c_p, and k represent the salt density, specific heat capacity, and thermal conductivity, respectively. Equation (8) is subjected to appropriate initial and boundary conditions. For the cavern walls, in particular, a Robin-type boundary condition is applied, where the heat diffusion equates to the convective heat transfer between the cavern walls and the fluid stored in the cavern.

Linear momentum balance equation

The linear momentum balance equation for quasi-static loading can be expressed as

$$\nabla \cdot \boldsymbol{\sigma} = \rho \mathbf{g}, \tag{9}$$

with $\mathbf{g}$ representing the acceleration vector. The stress tensor is given by Hooke's law, that is,

$$\boldsymbol{\sigma} = \mathbf{C} : (\boldsymbol{\varepsilon} - \boldsymbol{\varepsilon}_{ne} - \boldsymbol{\varepsilon}_{th}), \tag{10}$$

where $\mathbf{C}$ is the elastic stiffness tensor, $\boldsymbol{\varepsilon}_{th}$ and $\boldsymbol{\varepsilon}_{ne}$ are the thermoelastic and non-elastic strains (both addressed in the next section), and $\boldsymbol{\varepsilon}$ is the total strain tensor, given by $\boldsymbol{\varepsilon} = \nabla_s \mathbf{u}$ for infinitesimal strains. In addition, to boundary conditions, Eq. (9) is also time dependent due to creep deformations, so initial conditions must also be provided.

Cavern abandonment model

Cavern abandonment usually consists in filling the cavern with brine, let it rest for thermal equilibrium, and shut it in. In this situation, although the initial brine pressure (i.e., immediately after shut-in) is known, the evolution of brine pressure over time will be a result of cavern volumetric convergence. The evolution of cavern convergence, in turn, also depends on the brine pressure. To solve this coupled problem, an iterative boundary condition is applied to the momentum balance equation, in which brine pressure is calculated based on the cavern volume of the previous iteration, and applied as a normal load (Neumann) on the cavern walls to obtain a new cavern volume. This iterative process is repeated until the error is below a pre-specified tolerance within a certain time step.

In the iterative process described above, two steps must be carefully executed and implemented in the simulator. The first one refers to the brine pressure computation based on volumetric variations, while the

second is the accurate computation of the cavern volume. The next two subsection describe these two steps.

Brine thermodynamic model

In this work, brine is assumed to be in thermal equilibrium with the salt rock mass. The isothermal compressibility is defined as

$$c_b := -\frac{1}{V}\left(\frac{\partial V}{\partial p}\right)_T, \tag{11}$$

where p is brine pressure and V is the cavern volume. Integrating Eq. (11) between two consecutive time steps, that is, from p^t to $p^{t+\Delta t}$ and from V^t to $V^{t+\Delta t}$, leads to

$$p^{t+\Delta t} = p^t + \frac{1}{c_b}\ln\left(\frac{V^t}{V^{t+\Delta t}}\right). \tag{12}$$

Cavern volume

The volume of the cavern must be calculated at each new iteration of the simulation, thus many times within the same time step. The volume calculation process is partially illustrated in Fig. 4. The first step is to choose a point along the cavern centerline (point A). This point A is then connected to the vertices B, C, and D of one of the triangles on the cavern wall, forming a tetrahedron with a certain volume. Keeping point A as a reference point, this process is repeated for all triangles on the cavern wall, and the volumes of the corresponding tetrahedra are calculated and added together to give the total volume of the cavern. In this manner, the cavern volume computation can be expressed as

$$V = \frac{1}{6}\sum_{i=1}^{N_{tri}}\left(r_{i,B} - r_A\right)\cdot\left(r_{i,C} - r_A\right)\times\left(r_{i,D} - r_A\right), \tag{13}$$

where N_{tri} is the number of triangles on the cavern wall, r_A is the position vector of point A, and $r_{i,B}$, $r_{i,C}$, and $r_{i,D}$ are the position vectors of points B, C, and D of triangle i. The position vectors of each vertex are updated based on the displacement solutions during the simulation.

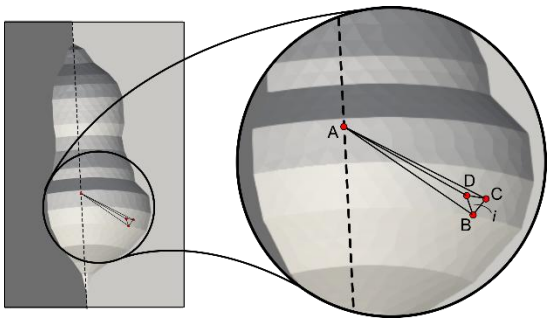

Figure 4 - Illustration of the strategy adopted to calculate the cavern volume.

Implementation and numerical formulations

The models described above are implemented in the SafeInCave simulator, an open-source 3D finite element package specifically designed for simulating the mechanical behavior of salt caverns during operation (storage) and after abandonment. The source code is public available at our GitLab repository and the documentation can be found here. The SafeInCave simulator is written in Python language, and uses many external packages, such as:

- FEniCSx (Baratta *et al.*, 2023) for the finite element implementation;
- *mpi4py* (Rogowski *et al.*, 2023) for parallelization;
- *petsc4py* (Dalcin *et al.,* 2011) for advanced Krylov solvers and preconditioners;
- *Pytorch* (Paszke *et al., 2019*) for efficient vectorized operations;

- *meshio* (Schlömer, 2024) for handling mesh formats;
- among others.

The constitutive models for salt rock render the momentum balance equations to be non-linear. We adopt a linearization procedure by obtaining a consistent tangent matrix, independently of the constitutive model employed. In this manner, a robust formulation is obtained at the same time as flexibility is maintained. For time discretization, the user can choose between explicit, Crank-Nicolson, and fully-implicit (i.e., backward Euler scheme).

Results

In this section, we present results obtained with the SafeInCave simulator to illustrate some of its capabilities in extracting insights of the mechanical behavior of salt caverns.

Test case 1: Validation and calibration

In this test case, we validate the constitutive model against a triaxial test, and evaluate the impact of model calibration at both lab and field scale. The constitutive model employed includes an elastic spring, a viscoelastic element (reverse transient creep), a viscoplastic element (transient creep), and a dashpot to represent dislocation creep. Therefore, the total strain is given by

$$\boldsymbol{\varepsilon} = \boldsymbol{\varepsilon}_e + \boldsymbol{\varepsilon}_{ve} + \boldsymbol{\varepsilon}_{vp} + \boldsymbol{\varepsilon}_{dc}.$$

For the lab scale validation, a unitary cube is subjected to the axial and radial (confining pressure) loads illustrated in Fig. 2. For the field scale analysis, a salt cavern simulation is performed on the geometry depicted in Fig. 5, where the side and overburden are also shown, and the gas pressure is applied in a cyclic manner, always within the envelope of 20% to 80% of lithostatic pressure at the cavern's roof.

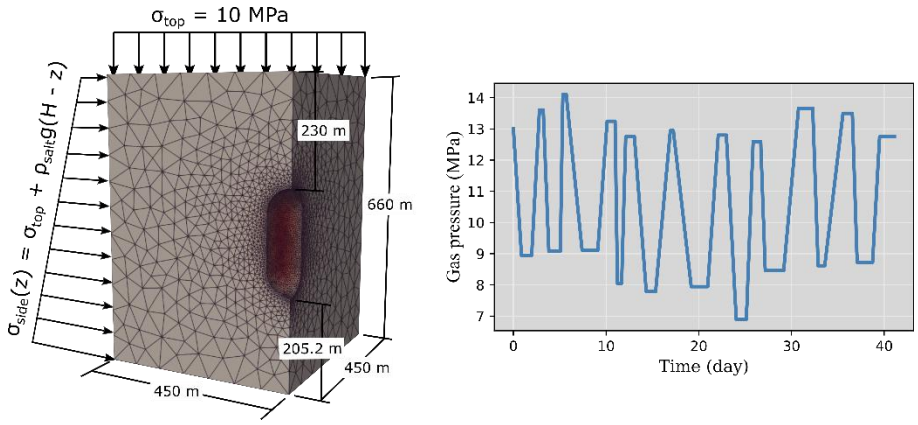

Figure 5 - Geometry and boundary conditions for test cases 1 and 2.

Manual calibration is performed for finding material parameters that can fit the experimental ε_1 and ε_3 shown in Fig. 2. Through this calibration process, we were able to find to different sets of material parameters, named Salt-A and Salt-B, that could produce a good fit (the reader can check these material parameter sets in Honório & Hajibeygi, 2024). The results are presented in Fig. 6-a, which also show that the mean absolute percentage error (MAPE) are about the same for both sets of material parameters. This suggests that using either Salt-A or Salt-B should produce similar results in salt cavern simulations. However, this is not the case, as shown by the results of cavern volumetric loss (convergence) presented in Fig. 6-b. These results emphasize that model calibration should not be taken lightly, and obtaining good results against one laboratory experiment is not enough to ensure predictability. Ideally, model calibration should include as much experiments as possible (Honório *et al.,* 2024).

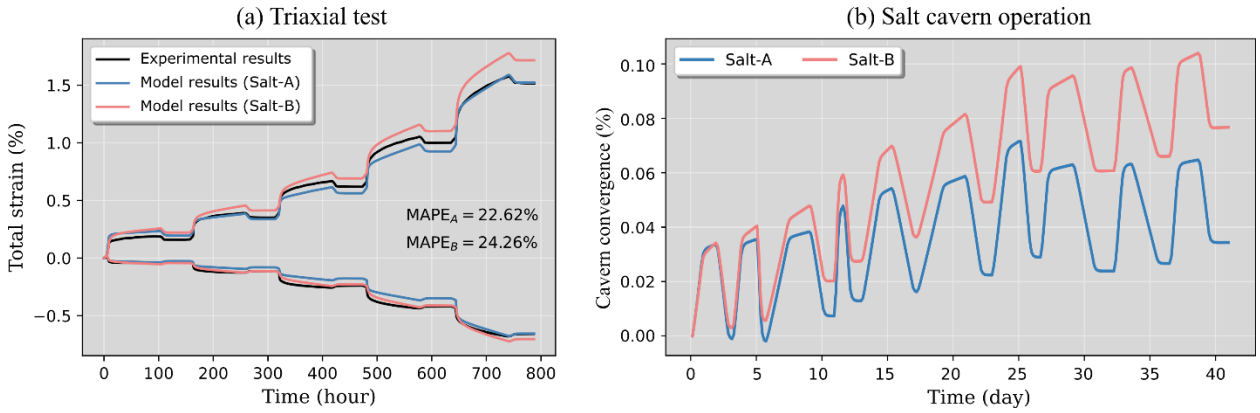

Figure 6 - (a) Model validation against triaxial test, and (b) simulation of cavern volumetric loss.

Test case 2: Impact of transient creep

Including the viscoplastic element (Desai's model) to describe transient creep is essential for the model to adequately fit the experimental triaxial results, as shown in Fig. 6-a. This suggests that including transient creep in salt cavern simulations is equally important. In order to test this hypothesis, we solve the same problem depicted in Fig. 5 with two different models: Model A includes an elastic spring, viscoplasticity (transient), viscoelasticity (reverse) and dislocation creep; and Model B is the same as Model A, but without viscoplasticity (i.e., transient creep). That is,

$$\text{Model A:} \qquad \boldsymbol{\varepsilon} = \boldsymbol{\varepsilon}_e + \boldsymbol{\varepsilon}_{ve} + \boldsymbol{\varepsilon}_{vp} + \boldsymbol{\varepsilon}_{dc}$$

$$\text{Model B:} \qquad \boldsymbol{\varepsilon} = \boldsymbol{\varepsilon}_e + \boldsymbol{\varepsilon}_{ve} + \boldsymbol{\varepsilon}_{dc}.$$

The left graph in Fig. 7-a shows the resulting cavern convergence obtained with the two models. As it can be verified, Model A produces higher volumetric losses in the few cycles, but the difference between the two models tend to vanish with time. The explanation for this lies in the resulting stress field. The right graph in Fig. 7-a shows the stress path obtained with Models A and B at a certain point on the cavern wall. It shows that, in the first few cycles, the obtained von Mises stress (which is proportional to $\sqrt{J_2}$) tend to be higher for Model B. This means that, although the total strains are higher for Model A, due to the presence of viscoplasticity, the dislocation creep element in Model B perceives higher stresses during the first few cycles. As a result, the strain rate due to dislocation creep in Model B is higher than in Model A, thus allowing Model B to "catch up" with Model A.

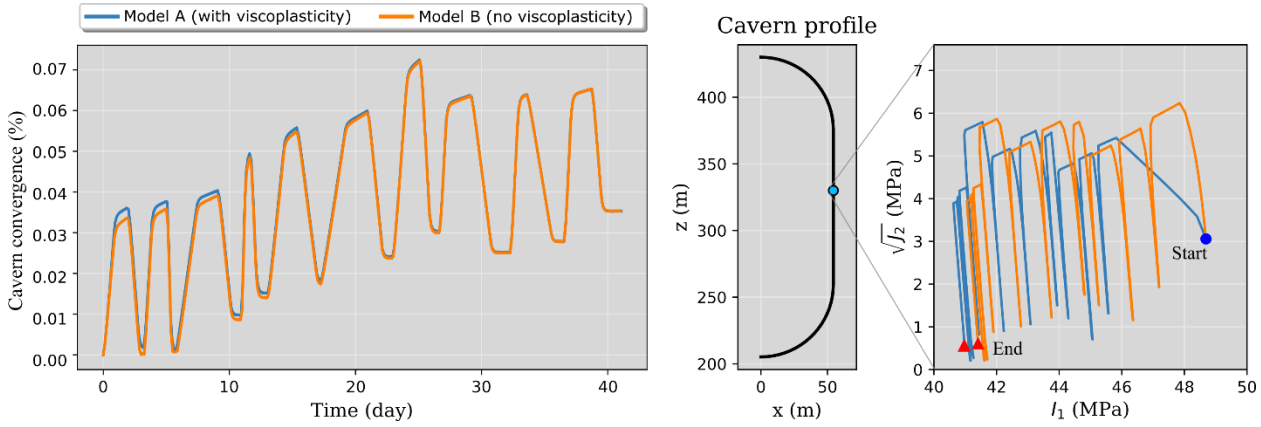

Figure 7 – Impact of transient creep: comparisons between Models A and B.

Test case 3: Impact of pressure solution

In this test case, the relative impact of pressure solution is investigated for salt cavern operations at different depths. The base geometry is illustrated in Fig. 8, as well as the temperature profile. All boundaries are prevented from normal displacement, except for the top boundary, which can freely move, and the cavern wall. The gas pressure imposed on the cavern wall varies from 20 to 80% of the local lithostatic pressure, and the simulation is run for 100 days.

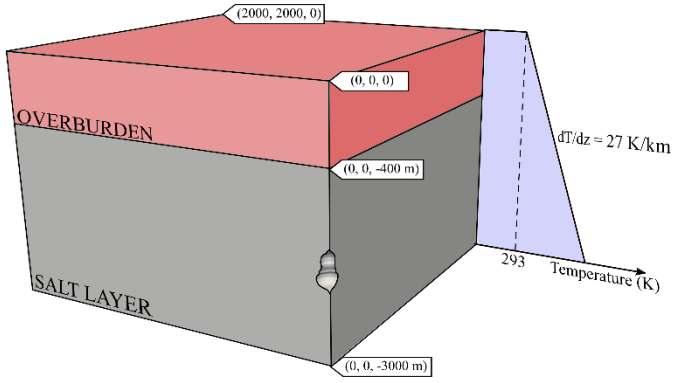

Figure 8 - Geometry and temperature profile used for test cases 3 and 4.

Two cavern depths are considered: 750 m (shallow) and 1300 m (deep). For each cavern depth, simulations are performed with and without pressure solution creep, while elasticity and dislocation creep are considered in all cases. The volumetric convergence of the cavern is monitored over time, and the relative differences between the cases with and without pressure solution creep for the two depths are shown in left graph of Fig. 9. It shows that the impact of including pressure solution creep in the constitutive model is bigger for shallow caverns. This is explained by the fact the von Mises stresses are higher for deeper caverns, as shown in the right images of Fig. 9, which causes dislocation creep to dominate. On the other hand, the lower von Mises stresses in the shallow cavern cause pressure solution and dislocation creep to be more comparable with each other, hence the higher importance of pressure solution in shallow caverns.

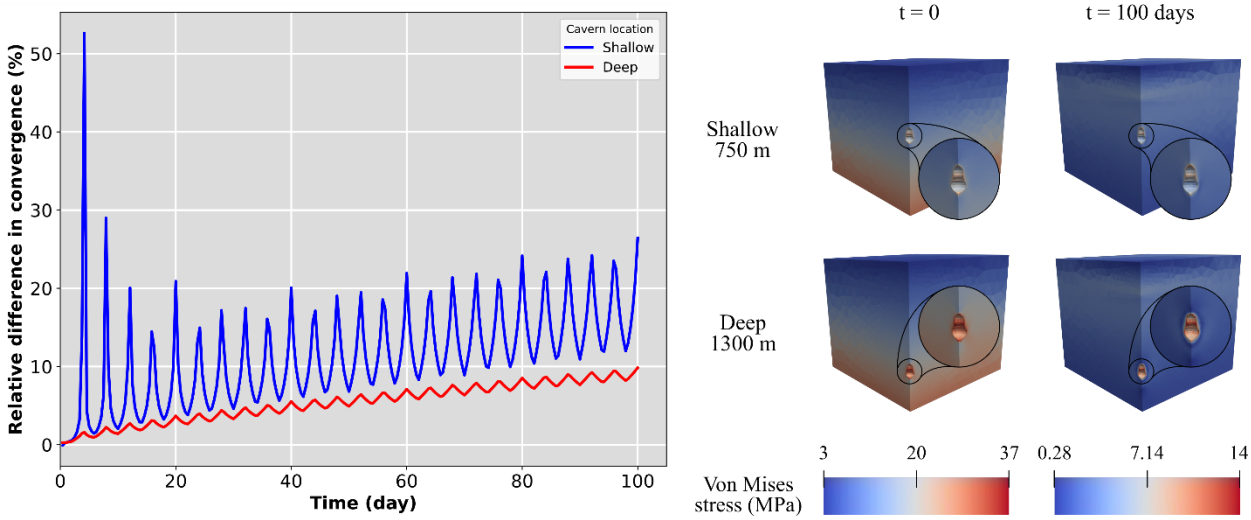

Figure 9 - (Left) Relative difference in cavern convergence due to the presence of pressure solution creep. (Right) Von Mises stress fields at initial and final time for deep and shallow caverns.

Test case 4: Cavern abandonment

For the cavern abandonment test case, the same setup depicted in Fig. 8 is employed. For simplicity, the constitutive model only considers elastic and dislocation creep strains, that is, $\boldsymbol{\varepsilon} = \boldsymbol{\varepsilon}_e + \boldsymbol{\varepsilon}_{dc}$. The different

scenarios consist of the same cavern shape abandoned at different depths, from 600 m to 2000 m. The abandonment strategy consists of hard shut-in (Buzogany *et al.,* 2022), and the initial brine pressure is always equal to the local wellhead pressure at the cavern roof, p_{wh}. The normalized brine pressure is analyzed over time, which is defined as

$$p_{\mathrm{norm}}(t) = \frac{p_{\mathrm{brine}}(t) - p_{\mathrm{wh}}}{p_{\mathrm{litho}} - p_{\mathrm{wh}}},$$

where p_{litho} is the lithostatic pressure at cavern roof.

The left graph in Fig. 10 shows the behavior of the normalized brine pressure over time for different cavern depths, as well as the normalized lithostatic pressure for reference. It shows that brine pressure increases much faster for deeper caverns than for shallower caverns during the first year after abandonment. However, this trend reverses in the long-term, with the normalized brine pressure for deeper caverns almost stabilized way below the normalized lithostatic pressure. Conversely, the normalized brine pressure for the shallowest cavern surpasses the deeper cavern brine pressure about one year after abandonment and reaches values much closer to the lithostatic limit. The explanation for this comes from the way the von Mises stress field develops according to the cavern depth. The right images in Fig. 10 show the von Mises stress fields for two cavern depths (800 m and 2000 m) and for beginning and end (300 years) of the simulation. Overall, at the beginning of the simulation (t=0), the deepest cavern experiences the highest stresses, thus favoring faster cavern convergence and brine pressure increase. However, it is also observed that these higher von Mises stresses are relieved (decay) faster in deeper caverns, such that, after a relatively short period, the stresses are higher in the shallowest caverns. This is the reason brine pressure increases faster in shallower caverns in the long-term.

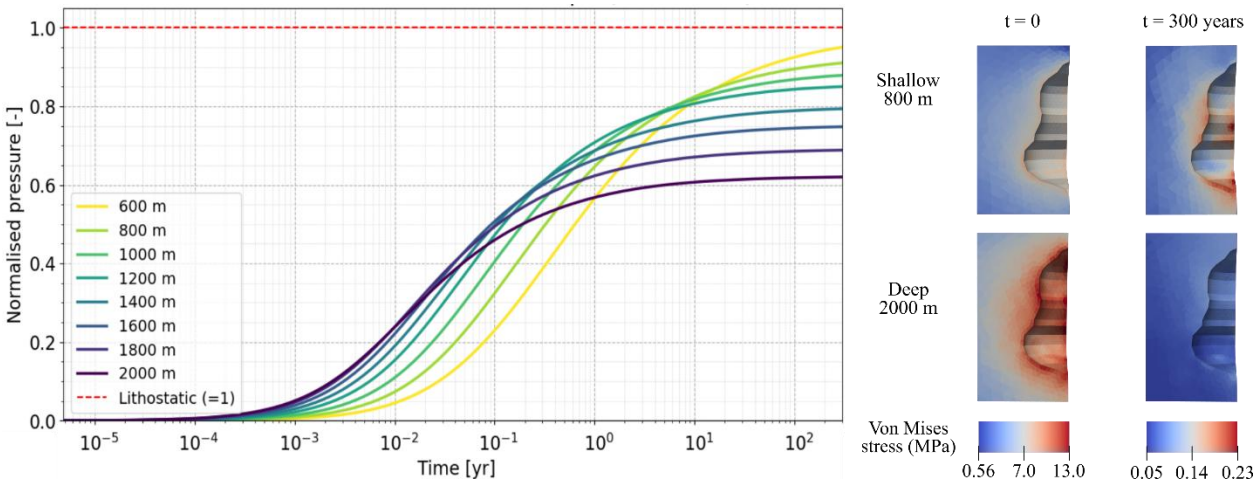

Figure 10 - Brine pressure evolution for different cavern depths.

Test case 5: Impact of thermal strains

The geometry shown in Fig. 8 is used again to test the effect of adding thermal strains to salt cavern simulations. For this purpose, the heat diffusion equation is solved on the same domain, with the outer (planar vertical) boundaries isolated, prescribed temperature on the top surface (298 K), pressure gradient (27 K/km) prescribed at the bottom, and convective heat flux imposed on cavern walls. The gas pressure and gas temperature are illustrated in Fig. 11. The problem is simulated with two models:

Thermal: $\boldsymbol{\varepsilon} = \boldsymbol{\varepsilon}_e + \boldsymbol{\varepsilon}_{dc} + \boldsymbol{\varepsilon}_{th}$

No-thermal: $\boldsymbol{\varepsilon} = \boldsymbol{\varepsilon}_e + \boldsymbol{\varepsilon}_{dc}$

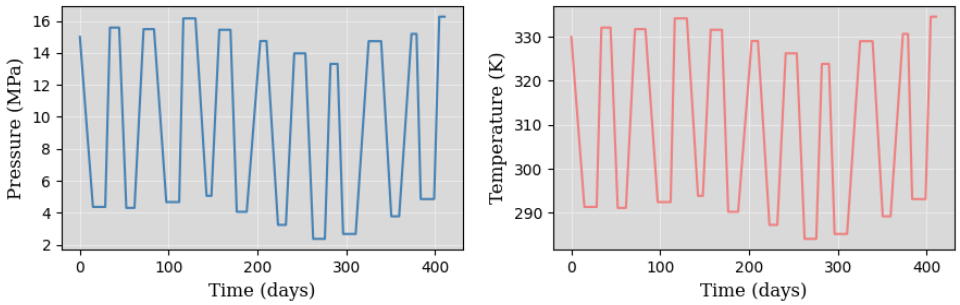

Figure 11 - Gas pressure and gas temperature over time.

The problem is simulated for 400 days, and the results are shown in Fig. 12. The left diagram indicates the point around the cavern where the stresses are monitored over time. The von Mises and mean stresses at the probing point are shown in the middle and right graphs of Fig. 12. It can be observed that the presence of thermal strains does not affect the von Mises stress significantly, which suggests that dislocation creep, and hence cavern convergence, is also not impacted. The mean stress, on the other hand, seems to be increased when thermal strains are included. However, this is not expected to cause any relevant impact on the mechanical stability of the salt cavern.

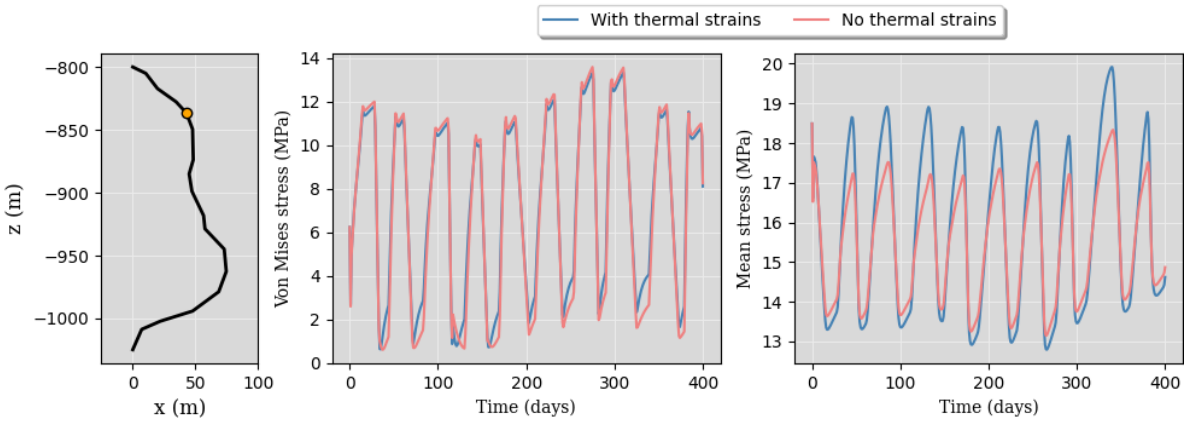

Figure 12 - Von Mises and mean stress with and without thermal strains.

Conclusions

This paper presented the capabilities of SafeInCave, an open-source 3D finite element simulator designed to simulate the thermos-mechanical behavior of salt caverns. The physical models included allow for simulation of storage operations, with fast cyclic storage, as well as cavern abandonment, with an isothermal thermodynamic model for brine. Moreover, the numerical implementation allows for easily changing between different constitutive models, while ensuring robustness.

Acknowledgements

This work was sponsored by Shell Global Solutions International B.V, and currently supported by Energi Simulation and SHINE project.

References

Honório, H. T., Houben, M., Bisdom, K., van der Linden, A., de Borst, K., Sluys, L. J., & Hajibeygi, H. (2024). A multi-step calibration strategy for reliable parameter determination of salt rock mechanics constitutive models. *International Journal of Rock Mechanics and Mining Sciences*, *183*, 105922.

Desai, C. S., & Varadarajan, A. (1987). A constitutive model for quasi-static behavior of rock salt. *Journal of Geophysical Research: Solid Earth*, *92*(B11), 11445-11456.

Khaledi, K., Mahmoudi, E., Datcheva, M., & Schanz, T. (2016). Stability and serviceability of underground energy storage caverns in rock salt subjected to mechanical cyclic loading. *International journal of rock mechanics and mining sciences*, *86*, 115-131.

Honório, H. T., & Hajibeygi, H. (2024). Three-dimensional multi-physics simulation and sensitivity analysis of cyclic energy storage in salt caverns. *International Journal of Hydrogen Energy*, *94*, 1389-1405.

Spiers, C. J., Schutjens, P. M. T. M., Brzesowsky, R. H., Peach, C. J., Liezenberg, J. L., & Zwart, H. J. (1990). Experimental determination of constitutive parameters governing creep of rocksalt by pressure solution. *Geological Society, London, Special Publications*, *54*(1), 215-227.

I. A. Baratta, J. P. Dean, J. S. Dokken, M. Habera, J. S. Hale, C. N. Richardson, M. E. Rognes, M. W. Scroggs, N. Sime, and G. N. Wells. DOLFINx: The next generation FEniCS problem solving environment, *preprint* (2023).

M. Rogowski, S. Aseeri, D. Keyes, and L. Dalcin, *mpi4py.futures: MPI-Based Asynchronous Task Execution for Python*, IEEE Transactions on Parallel and Distributed Systems, 34(2):611-622, 2023. https://doi.org/10.1109/TPDS.2022.3225481

Paszke, A., Gross, S., Massa, F., Lerer, A., Bradbury, J., Chanan, G., ... & Chintala, S. (2019). Pytorch: An imperative style, high-performance deep learning library. *Advances in neural information processing systems*, *32*.

Schlömer, N. Meshio: Tools for Mesh Files. v5.3.5, Zenodo, 31 Jan. 2024, https://doi.org/10.5281/zenodo.1288334.

Buzogany, R., Zander-Schiebenhöfer, D., Wijermars, E., & den Hartogh, M. (2022). Development of surface deformations above salt caverns depending on the abandonment scenario. In *The Mechanical Behavior of Salt X* (pp. 553-566). CRC Press.

L. Dalcin, P. Kler, R. Paz, and A. Cosimo, *Parallel Distributed Computing using Python*, Advances in Water Resources, 34(9):1124-1139, 2011. https://doi.org/10.1016/j.advwatres.2011.04.013